Journal of The Electrochemical Society, 2021 **168** 030529

On the Solvation of Redox Mediators and Implications for their Reactivity in Li-Air Batteries

Erlendur Jónsson,[1,=] James H. J. Ellison,[1,=] Evelyna Wang,[1] Vera Kunz,[1] Tao Liu,[2] Israel Temprano,[1,z] and Clare P. Grey[1,*,z]

[1]*Department of Chemistry, University of Cambridge, Cambridge, United Kingdom*
[2]*Shanghai Key Laboratory of Chemical Assessment and Sustainability, Department of Chemistry, Tongji University, Shanghai, People's Republic of China*

Lithium-air batteries are a promising energy storage technology for transport applications, given their exceptionally high energy density. However, their development is significantly hampered by high overpotentials, which lead to poor efficiency and short lifetimes. Redox mediators provide a solution to this problem by shuttling electrons from the electrode to the active species at just above the redox potential of the mediator. Thus, knowing the redox potential and having the ability to tune it are critical to electrochemical performance. We focus on LiI as a model mediator—given its additional role in controlling LiOH vs Li_2O_2 chemistry—and use cyclic voltammetry (CV), NMR, UV/Vis spectrometry, and molecular dynamics (MD) simulations to monitor the effects of electrolyte composition on solvation. Li^+ and I^- solvation in common Li-air solvents, the electrochemical implications, and the applicability of each technique to probe the nature of the solvation shell and its effect on the electrochemical properties are explored. Starting with a simple thermodynamic model, we then used UV/Vis spectrometry to probe I^- solvation, ^1H NMR spectroscopy to study water solvation and ^{31}P of the probe molecule triethylphosphine oxide (TEPO) to explore Li^+ solvation; we find that no single descriptor can provide an accurate description of the solvation environment. Instead, we use all these methods in combination with the MD results to help rationalise the CV data. We find that the I^- solvation improves significantly in tetraglyme (G4), with increasing salt and water concentration, but minimal effects on changing salt/water concentrations are seen in DMSO. In contrast, increasing salt concentration increases the Li^+ activity in DMSO but not in G4. Furthermore, a simple model considering the equilibria between the different species was used to explain the ^1H NMR data.
 [DOI: 10.1149/1945-7111/abeb26]

Manuscript submitted November 25, 2020; revised manuscript received February 5, 2021. Published March 18, 2021. *This paper is part of the JES Focus Issue on Selected Papers of Invited Speakers to IMLB 2020.*

Supplementary material for this article is available online

Secondary Li-air batteries (LABs), with their high theoretical capacity (~3500 Wh kg^{-1}), are a promising alternative to lithium-ion batteries (LIBs) for applications where energy density is the primary concern.[1–4] The development of secondary batteries with such high energy densities is a highly desirable target, as commitments that restrict the use of fossil fuels in transport applications are increasingly becoming adopted worldwide.[5,6] The development of LABs is still, however, at an early stage and multiple fundamental challenges need to be overcome to produce commercially viable devices.[3,4] Amongst these challenges, the high charge overpotential and the consequent degradation of cell components is one of the most difficult to tackle, despite many efforts in this area.[2] The use of redox mediators (RMs), chemical species that facilitate electron transfer between the solid, electron-conducting component of the cathode(i.e., the air side), and the active species either in the solution or at the surface of solid precipitates (where they are not in direct electrical contact with the electrode), is currently considered amongst the most promising strategies to overcome some of these challenges.[7–11]

Multiple RMs have been used to assist with both the oxygen reduction (ORR) and oxygen evolution reactions (OER) in LABs.[7–11] These reactions take place with the electrode polarised just above the mediator's half-wave potential (or redox couple) ($E(RM^{red}/RM^{ox})$), thus reducing overpotentials and side reactions.[9–11] The selection of a RM is a complex process as it must be chemically and electrochemically stable, have fast electrode kinetics, and possess appropriate redox couples to mediate the charge and/or discharge reactions. The redox couple dictates the charge/discharge voltage during galvanostatic cycling and hence largely determines the energy efficiency.

There is a tendency in the literature to refer to the redox couple of a RM as a unique and fundamental property, despite the well-documented observations that the electrolyte in which the RM operates influences its value,[12,13] with the large shift in the couple in moving from aqueous to non-aqueous electrolytes being the most well-established occurrence of this phenomenon. Pande and Viswanathan discussed this effect, arguing that since the Gibbs free energy of a particular species in solution ($\Delta_{sol}G$) is primarily dependent on the interactions in its first solvation shell, these interactions ought to influence the equilibrium of redox couples.[14] The interactions in the solvation shell are different depending on the nature of the RM. According to their charge in the reduced and oxidized states, RM can be classed into four different types:

I. $RM^{m+} + me^- \rightleftarrows RM$
II. $RM + me^- \rightleftarrows RM^{m-}$
III. $RM^{n+} + me^- \rightleftarrows RM^{(n-m)+}$
IV. $RM^{n+} + me^- \rightleftarrows RM^{(n-m)-}$

Recently, several studies have investigated the effect of physicochemical parameters of the electrolyte (solvent acceptor/donor number, salt concentration, etc.) on the measured redox potentials of the I^-/I_3^- pair, a commonly used RM in Li-O_2 cells,[12,13] and their influence on its ability to mediate the decomposition of various discharge products (Li_2O_2 and LiOH).[15,16] It has been shown that the $E(I^-/I_3^-)$ can vary by as much as 0.6 V depending on the electrolyte.[12,13,15,17] To illustrate this variation, we have plotted the observed $E(I^-/I_3^-)$ in some recent studies using the most common solvents in Li-O_2 cells, i.e. ethylene glycol dimethyl ether (G1), tetraethylene glycol dimethyl ether (G4), and dimethyl sulfoxide (DMSO), as a function of the total [Li^+] (Fig. 1).[11–13,17–21]

According to the general principle outlined by Viswanathan and co-workers[14] and as recently discussed by several groups in the particular case of LiI,[12,13,15] the solvent acceptor/donor number (AN/DN) and [Li^+] contribute to the variations in $E(I^-/I_3^-)$.

[=]These authors contributed equally to this work.
[*]Electrochemical Society Fellow.
[z]E-mail: cpg27@cam.ac.uk; it251@cam.ac.uk

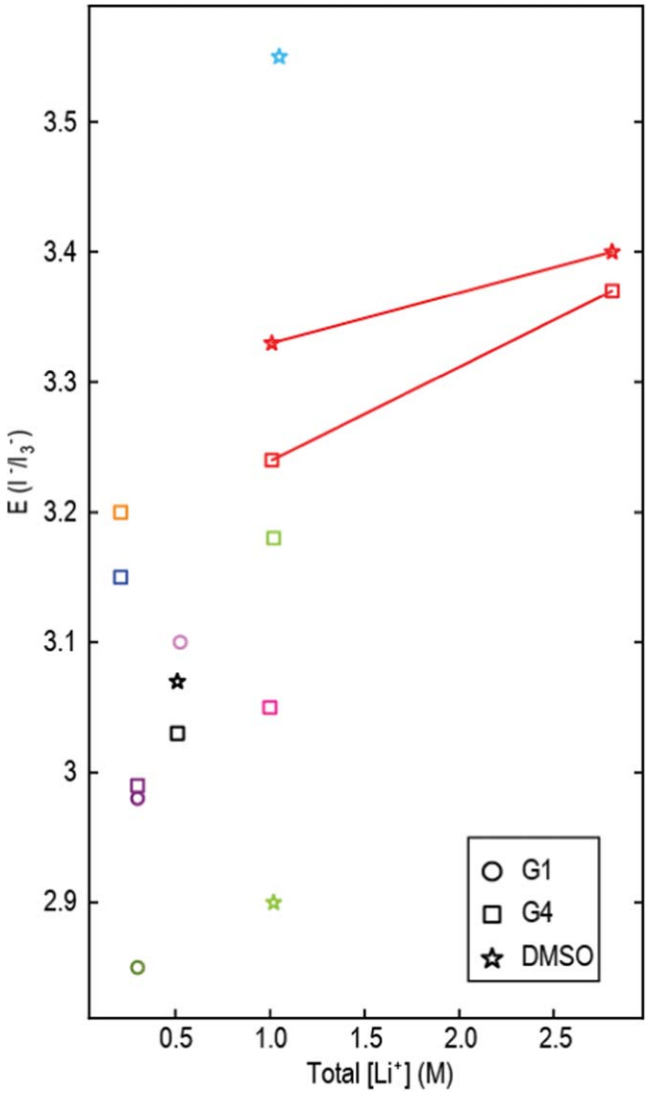

Figure 1. Variations of the reported redox equilibrium potential of the I^-/I_3^- couple vs the Li/Li^+ couple as a function of the total $[Li^+]$; colours are used to distinguish between studies (black;[12] purple;[11] red;[13] blue;[21] green;[20] pink;[19] orange;[18] bright green[17]). Data points from the same study are connected with a line.

However, the correlation between a single characteristic, as Fig. 1 illustrates for $[Li^+]$, and the redox potential does not capture the whole picture, as the factors affecting the solvation sphere of I^- are multidimensional in nature and difficult to assess. In particular, the change in AN of the solvent has often been used in the literature as a proxy for the shift in $E(I^-/I_3^-)$, as solvents with higher AN solvate the I^- ion more effectively. However, as Fig. S1b (available online at stacks.iop.org/JES/168/030529/mmedia) shows (particularly for DMSO), a large scatter of values has been observed for each AN value, and thus it cannot be used to predict the redox potential of the I^-/I_3^- pair in isolation. Neither does $[Li^+]$ in isolation; with DMSO as the solvent (Fig. 1), Zhang et al.[20] report an $E(I^-/I_3^-)$ of 3.18 V in cells with 1 M LiTFSI and 20 mM LiI, the values shifting to 3.33 V in cells also containing 1 M LiTFSI but only 10 mM LiI in the studies of Nakanishi et al.;[13] Yu et al.[22] find an even higher value of $E(I^-/I_3^-) = 3.55$ V in cells containing 1 M $LiClO_4$ and 5 mM I_2 (all vs Li/Li^+).

In a recent study, we demonstrated that the introduction of additives that strongly solvate I^- can be used to increase $E(I^-/I_3^-)$, which in turn can activate different routes for LiOH electrooxidation.[15] We also observed that the competing solvation effects from different electrolyte components are difficult to model and thus more detailed studies to understand how the solvation shell of I^- affects the redox properties are needed.

In this work, we take LiI as a case study to examine how the physicochemical properties of the electrolyte containing I^-, vary for different solvents as a function of [LiTFSI] and $[H_2O]$. We focus on the addition of water to Li-air battery electrolytes, in part because water has been reported to increase discharge capacities by encouraging the growth of larger particles on discharge. Furthermore, it would be advantageous for a practical Li-air battery to utilise atmospheric air, which will enviably lead to some moisture entering the cell. It is thus important to understand the effect of water on the electrochemistry. Additionally, the presence of water in the cell will likely lead to the formation of some LiOH as a discharge product. Delving deeper into our previous findings,[15] here we start by discussing the general thermodynamic considerations that influence the redox-mediated OER process (for both Li_2O_2 and LiOH chemistries) and highlight the importance of the RM solvation to these considerations. Next, and again following on from our previous observation that the activity of I^- is strongly dependent on the nature of its solvation,[15] we use CV, NMR, UV/Vis and molecular dynamics (MD) simulations to investigate the solvation characteristics of I^- in commonly used electrolyte mixtures in Li-O_2 cells as a function of lithium salt concentration, water concentration, and solvent. We explore how the AN is determined for each solvent. Based on all these results, we attempt to rationalise the effect of various interactions with electrolyte components to the solvation, and therefore activity of I^-, and we further discuss the considerations that need to be taken into account when using the different characterization techniques. We conclude that no one method gives complete information on the system nor do they always give direct information on the thermodynamics and often require careful interpretation. Therefore, a holistic approach is required to obtain an accurate understanding of how different electrolyte components affect the solvation of iodide, and the large variation in the I^-/I_3^- redox potential observed in the literature.

Experimental

Materials.—Electrolytes based on three different solvents, DMSO, G1, and G4 were prepared with 50 mM LiI. G1 and G4 (Aldrich, 99%) were heated with sodium metal under Ar for 3 d prior to fractional distillation. The final water content was measured by Karl Fischer titration (Metrohm) at <50 ppm and then stored over 4 Å molecular sieves. LiTFSI (3 M) and LiI (Aldrich, 99.9%) were dried in vacuo at 160 °C and 200 °C, respectively, for 12 h before being used to prepare the electrolyte.

Cyclic voltammetry (CV).—CV experiments were recorded in a custom-made glass cell, using a glassy carbon working electrode (diameter 3 mm), a coiled platinum wire counter electrode, with a Ag/Ag^+ reference electrode. The Ag/Ag^+ reference electrode consisted of a silver wire immersed in 0.01 M $AgNO_3$ and 0.1 M Tetrabutylammonium perchlorate in acetonitrile. This reference solution was separated from the bulk solution by a glass frit. ^1H NMR was used to confirm that there was no significant leakage of acetonitrile into the bulk solution during the period of the measurements. CVs were conducted at 50 mV s^{-1} on a BioLogic VSP-300 Potentiostat over a varying voltage range. The range was adjusted to avoid spending excessive amounts of time above the I_3^-/I_2 oxidation potential to prevent electrolyte degradation. The reactions were conducted sequentially in order of decreasing concentration as described in Table SII. Each mixture was stirred for 2 min and then left to stand for 1 min between runs to ensure homogeneity. The half-wave potential was measured by taking the average of the peak current on the forward and backwards scans of the appropriate redox peak.

UV/Vis.—UV/Vis measurements were performed using an Avantes AvaSpec-Hs2048XL-EVO SenseLine detector and Ocean

Optics DH-Mini deuterium/halogen light source. Measurements were taken in a transmission mode with 2.5 ms integration times and averaging over 200 spectra. A quartz UV cuvette, purchased from Starna Scientific, with a very short (10 μm) pathlength was used to prevent absorption saturation due to the opacity of electrolyte solutions with 50 mM LiI concentrations. Before the measurements, the cuvette was flushed with EtOH, blow dried with N_2 gas, then under vacuo for 1 h and finally stored at 60 °C overnight.

NMR.—One-dimensional ^{1}H and ^{31}P{^{1}H} NMR spectra were recorded on a Bruker Avance Neo 400, [9.4 T] (ω^1H = 400 MHz) spectrometer using a BBO probe. ^{1}H spectra were internally referenced to C_6D_6 at 7.26 ppm (δ ^{1}H) in a capillary, which was also used for locking in both ^{1}H and ^{31}P spectra.

MD.—Simulation boxes were constructed with the same salt/solvent ratios as for the experimental part (the number of molecules simulated in each system are found in Table SVII) using Packmol.[23] The OPLS-AA force field was used as the basis for the simulations. Parameters for TFSI were taken from Canongia Lopes et al.[24] Virtualchemistry.org was helpful for DMSO parameters.[25] Gromacs 2020, along with its analysis toolchain, was used for all simulations.[26] Each simulation was set up as follows: a startup run of 0.1 ns NVT (Nosé-Hoover thermostat, time constant = 1 ps), 2 ns NPT run (Parrinello-Rahman barostat, time constant = 1 ps), followed by a 5 ns NVT production run. The time step of all simulations was 1 fs.

Results

Thermodynamic considerations.— *General redox mediator and Li_2O_2.*—In order to identify the key factors that affect the activity of redox mediators in Li-O_2 cells, we consider the thermodynamic driving force for the charge reaction between a general RM and Li_2O_2. We make the assumption that the solution is saturated with discharge product (that is, the ΔG_r of the dissolution of solid Li_2O_2 is zero) and at equilibrium with some partial pressure of oxygen gas (P_{O_2}). The oxygen evolution reaction (OER) is then described as:

$$Li_2O_2 \rightleftarrows 2\ Li + O_2 \quad [1]$$

which combines the reaction at the cathode

$$Li_2O_2 \rightleftarrows 2\ Li^+ + O_2 + 2\ e^- \quad [2]$$

with the reaction at the anode

$$2\ e^- + 2\ Li^+ \rightleftarrows 2\ Li \quad [3]$$

However, with a redox mediator present this reaction follows a two-stage catalytic mechanism, in which first the RM is electrochemically oxidised (the RM^{red}/RM^{ox} couple):

$$Li^+ + RM^{red} \rightleftarrows Li + RM^{ox} \quad [4]$$

Where the charges on RM^{red} and RM^{ox} differ by 1, for the one-electron process assumed here. Subsequently Li_2O_2 is chemically oxidised to O_2 by the oxidised mediator, RM^{ox} ($O_2^{2-} \rightarrow O_2$):

$$Li_2O_2 + 2\ RM^{ox} \rightleftarrows 2RM^{red} + O_2 + 2Li^+ \quad [5]$$

Reaction (4) is again a combination of the reaction at the cathode (6) and the anode (7)

$$RM^{red} \rightleftarrows RM^{ox} + e^- \quad [6]$$

$$Li^+ + e^- \rightleftarrows Li \quad [7]$$

It can be shown (see Eqs. 1–8 in the SI for detailed analysis) that the $\Delta_r G$ for reaction (1) is given by

$$\Delta_r G(O_2^{2-} \rightarrow O_2) = -\Delta_f G°(Li_2O_2) + kTln\left(\frac{P_{O_2}}{P°}\right) + 2FE(RM^{red}/RM^{ox}) \quad [8]$$

Recognising that this is the OER in the presence of the RM^{red}/RM^{ox} redox couple, we can see that there are two key variables dictating the driving force for the OER:

1. The redox equilibrium potential of the RM couple, $E(RM^{red}/RM^{ox})$
2. The oxygen partial pressure, P_{O_2}

Iodide-mediated LiOH cycling.—Recently, iodide-mediated cells with water-containing electrolyte have been studied in relation to the $4e^-/O_2$ formation/decomposition of LiOH. However, the reversibility of this process has been heavily questioned[11,12,17,27] due to the low equilibrium redox potential shown by the I^-/I_3^- couple in the electrolytes tested (below the potential of the OH^-/O_2 couple at standard conditions). Inour recent work,[15] we discussed the effect of the I^-/I_3^- equilibrium potential on the reversibility of LiOH-based cells and how the introduction of solvent additives that would regulate this potential was key. In order to assess the influence of $E(I^-/I_3^-)$ on the thermodynamics of the OER from LiOH electro-oxidation we consider the equilibrium:

$$4\ Li^+_{(sol)} + 4\ OH^-_{(sol)} \rightleftarrows 2\ H_2O_{(sol)} + O_{2(sol)} + 4\ Li_{(s)} \quad [9]$$

In the presence of an iodide redox mediator, this proceeds via the following two-stage catalytic mechanism, in which first I^- is oxidized to I_3^- (the I^-/I_3^- couple):

$$6\ Li^+_{(sol)} + 6\ I^-_{(sol)} \rightleftarrows 2\ Li^+_{(sol)} + 2\ I_3^-{}_{(sol)} + 4\ Li_{(s)} \quad [10]$$

Subsequently, LiOH is oxidised to O_2 by I_3^- with the regeneration of I^- ($OH^- \rightarrow O_2$):

$$4\ OH^-_{(sol)} + 2\ I_3^-{}_{(sol)} \rightleftarrows 6\ I^-_{(sol)} + 2\ H_2O_{(sol)} + O_{2(sol)} \quad [11]$$

It can be shown using similar logic to that used to derive Eq. 8 (see Eqs. 11–20 in the SI for detailed analysis) that:

$$\Delta_r G(OH^- \rightarrow O_2) = 2\Delta_f G°(H_2O) - 4\Delta_f G°(LiOH) + 4FE\left(\frac{I^-}{I_3^-}\right) + 2\Delta_{sol}G(H_2O) + kTln\left(\frac{P_{O_2}}{P°}\right) \quad [12]$$

This indicates that in the case of the iodide-mediated LiOH removal, there are three key variables that dictate the driving force for the OER:

1. The redox equilibrium potential of the I^-/I_3^- couple, $E(I^-/I_3^-)$
2. The free energy of water solvation, $\Delta_{sol}G(H_2O)$
3. The oxygen partial pressure, P_{O_2}

In both cases (Li_2O_2 and LiOH formation), the influence of the oxygen partial pressure is limited (estimated to ~0.08 eV per $4e^-$ reaction equivalent for the LiOH case[15] and ~0.08 eV per $2e^-$ reaction equivalent for Li_2O_2 case over a pressure range of 0.002 to 1.2 bar), whereas the redox equilibrium potential of the I^-/I_3^- couple has been observed to fluctuate between 2.9 and 3.6 V (vs Li/Li^+) as discussed above in the context of Fig. 1. [28] The influence of the water solvation term (in the LiOH formation case) is harder to evaluate. Estimations of the effect of the solvent[15] show that the water solvation term has an influence of ~0.17 eV under different conditions. In general, the high polarity and low dispersivity of water results in lower water activity in solvents which also have high

polarity and low dispersion. Additionally, the activity of water will be low in solvents that are good H-bond acceptors, since water is a very strong H-bond donor. However, these considerations can be significantly altered as salts are added to the solvent, since these can have a strong effect on the water's local co-ordination and hence its solvation, as shown below via ^{1}H NMR experiments.

In both the Li_2O_2 and LiOH cases, the spread in $E(I^-/I_3^-)$ is caused by the local electrolyte structure, as the voltage/free energy is proportional to the difference in solvation of RM^{red} and RM^{ox}:[28]

$$\Delta_r G(RM^{red}/RM^{ox}) \propto \Delta_{sol}G(Li^+) + \Delta_{sol}G(RM^{red}) - \Delta_{sol}G(RM^{ox}) \quad [13]$$

The free energy is also proportional to the solvation of the Li^+ ion, which defines the Li/Li^+ couple of the lithium anode. Understanding and being able to accurately predict these three solvation terms is thus of great importance to understanding the thermodynamics of the system and to enable refinement of the battery system. Although these solvation terms may prove difficult to evaluate due to the complex solvation shell, especially at higher salt and/or water concentrations, requiring an effective/average solvation environment, we use them as a theoretical starting point to aid discussion.

We first measure the I^-/I_3^- couple via CV for G4 and DMSO solvents as a function of water and [LiTFSI] concentration and then use a combination of measurements and MD simulations to help rationalise the changes. Specifically, we explore the $\Delta_{sol}G(RM^{red}) - \Delta_{sol}G(RM^{ox})$ terms using UV/Vis, and the $\Delta_{sol}G(Li^+)$ and $\Delta_{sol}G(H_2O)$ terms using NMR.

Cyclic voltammetry.—The I^-/I_3^- halfwave potentials extracted from the CV curves are given in Fig. 2 (CVs are found in Figs. S2 and S3 in SI). They were measured vs an Ag/Ag^+ reference due to the propensity of the Li/Li^+ couple to shift between different solvents. In G4-based electrolytes, increasing [LiTFSI] or $[H_2O]$ increases the I^-/I_3^- couple potential (by 55 mV from 500 mM to 2000 mM [LiTFSI], and 44 mV from 0 to 10,000 ppm water), indicating that I^- is becoming better solvated, relative to I_3^- (SI Eqs. 5 and 6). We ascribe this to the stronger interaction between the smaller I^- anion, with its higher charge/volume ratio, and the Li^+/or protons in water, with increasing $[H_2O]$ and [LiTFSI] resulting in stronger solvation of the I^- ion (relative to I_3^-). By contrast, in DMSO-based electrolytes, only a very small change was seen in the I^-/I_3^- redox couple in water containing mixtures as a function of [LiTFSI]. As DMSO is a more polar solvent than G4, it should better solvate I^-, rendering I^- ions essentially agnostic to the presence of Li^+ and H_2O. These hypotheses concerning the differences in I^- solvation will be explored below via experiment and theory.

For both DMSO and G4 these trends are broken at low salt concentrations, both showing a slight increase in the I^-/I_3^- couple. It seems unlikely that reducing the salt concentration would result in an improvement of the I^- solvation. We postulate that this may be due to *i*R effects—when the salt concentration becomes low and, the solution conductivity drops. As the forward scan has a larger current magnitude, this disproportionately affects the oxidation peak, causing an artificial increase in the I^-/I_3^- peak.

UV/VIS.—Halide ions in solution are known to absorb in the near-UV region, the energy of the excited state of the ion being dictated by the solvation environment.[29] This electronic transition is absent for the gas phase ion and is assigned to a charge-transfer process to (involving) the solvent.[29] Extensive work on these transitions in aqueous I^- solutions suggest that in the excited state, the promoted electron occupies an orbital constrained by the solvation shell and the iodine atom.[30,31] The absorption spectrum is therefore dependent on a variety of factors that affect the solvation environment of the iodide, such as solvent, concentration, added salts, and temperature.[32] While UV/Vis spectroscopy has been used in previous Li-O_2 battery studies to monitor the electrochemical behavior of LiI RM, it is typically used to simply compare the intensity of the I^- and I_3^- peaks, mainly to identify the redox species present during charge and discharge.[33] In this work, we specifically focus on the position of the I^- absorption peak, which reflects the solvation environment.

Clear changes in the I^- absorption peak are observed for the different electrolytes (Fig. 3a; full spectra shown in Fig. S4). When DMSO is used as the solvent, the I^- absorption peak at around

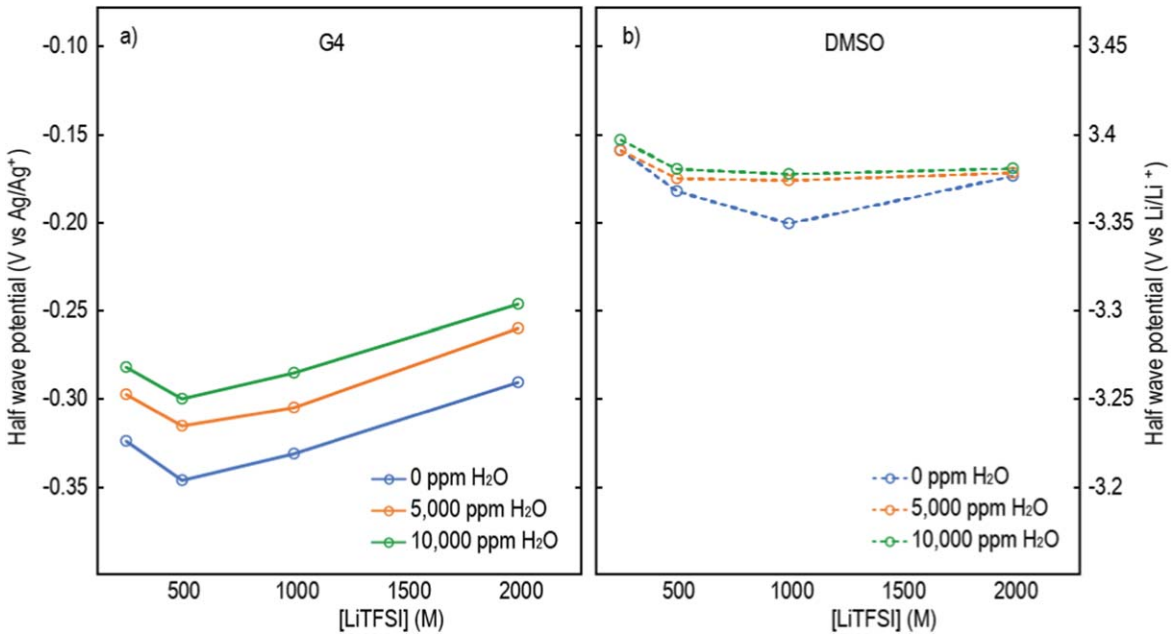

Figure 2. Half-wave potentials of the redox peaks assigned to the I^-/I_3^- couple as determined by CVs in (a) G4 and (b) DMSO as a function of [LiTFSI] with a scan rate of 50 mV s^{-1}. In each graph, three water concentrations are displayed, dry, 5,000 and 10,000 ppm. Measurements are taken vs an Ag/Ag^+ reference electrode using a glassy carbon working electrode and platinum wire counter electrode. For comparison, the scale on the right is the standard Li/Li^+ couple as estimated by an internal reference as described in the "Cyclic voltammetry" section of the SI.

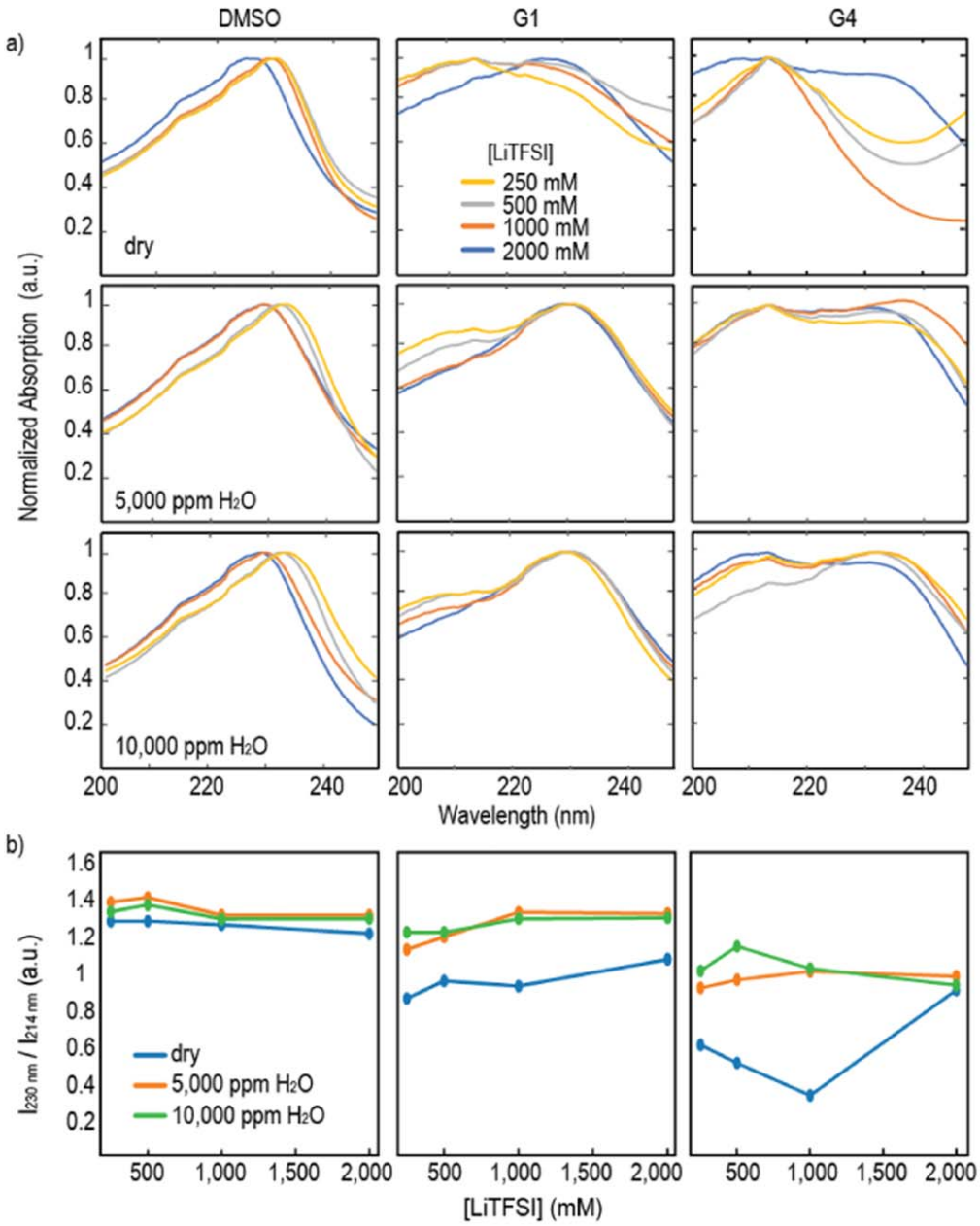

Figure 3. (a) UV absorption spectra in the 200–250 nm range corresponding to the absorption of I^- species in solution for various electrolytes: from left to right, DMSO, G1, and G4, and from top to bottom, neat electrolyte, 5,000 ppm water added, and 10,000 ppm water added at various salt concentrations ([LiTFSI]= 250 mM—yellow; 500 mM—grey; 1,000 mM—orange; 2,000 mM—blue). (b) Intensities of the absorption signals at 230 nm and 214 nm (corresponding to I^-) at different water concentrations (dry—blue; 5,000 ppm—orange; 10,000 ppm—green) as a function of [LiTFSI].

230 nm shifts slightly to shorter wavelengths, as [LiTFSI] is increased (Fig. S5). This is consistent with early reports on I^- solvation, which also indicate that increased numbers of alkali cations in the first I^- coordination shell increase the energy of the electronic transition.[34] This effect was attributed to a slight stabilization of the solvated I^- ground state due to the presence of alkali cations. In contrast, G1 and G4 electrolytes give rise to an absorption peak at 214 nm in neat electrolytes and a second peak at 230 nm peak appears only after the addition of either H_2O or at high [LiTFSI]. The presence of two distinct absorption peaks may be attributed to two solvation environments of the I^- species in these electrolytes, such as a coordination involving Li^+ vs onewithout. Furthermore, the presence of two environments suggests that water is not as uniformly dispersed in glymes as in DMSO, possibly due to clustering and hydrogen bonding at high water content.[16] This water clustering is discussed further in our ^{1}H NMR and MD sections.

Figure 3b shows a comparison of the relative intensities at 230 nm and 214 nm (I_{230nm}/I_{214nm}) for the different electrolytes in order to compare changes to these two peaks in the I^- absorption range. The largest change in the absorption spectra is seen on adding water to glyme electrolytes. The different behaviour of the I^- UV adsorption in glyme-based electrolytes compared to DMSO agrees with our hypothesis that the solvent polarity affects I^- solvation: In low polarity solvents, increased ion-pairring leads to more Li-I interactions, as compared to polar solvents such as DMSO and H_2O, where more dissociated ion-pairs are seen.[32] These findings align with work by Nakanishi et al., where they demonstrated that the effect of [LiTFSI] on LiI redox behaviour was greater in G4 than in DMSO.[13] Furthermore, G4 and DMSO interact with Li^+ ions in different ways, as later shown with ^{31}P NMR, which may also affect the subsequent solvation of I^- and the UV absorption.

Finally, the I_3^- absorption peak around 270 nm is not strongly affected by changing the electrolytes (see Fig. S4 in SI), in

agreement with our hypothesis that it is the I^- solvation that is more strongly affected by changes in the electrolyte.

NMR.—One potential direct probe of the iodine local environment would be ^{127}I NMR, which is a 100% abundant NMR active nucleus. However, the large quadrupolar interactions associated with the ^{127}I nucleus yield too broad a signal in all but the most symmetric coordination environments, rendering ^{127}I NMR impractical. Instead, we focus on two different NMR nuclei to study the effect of the electrolyte on the I^- solvation shell. The first method consists of adding a probe molecule to the electrolyte, the Lewis base, triethylphosphine oxide (TEPO)[35] and then measuring the ^{31}P NMR. This is the method used in the literature to determine the acceptor number.[12,36–39] The second method probes the electrolyte components directly by measuring the ^1H NMR.

^{31}P NMR.—The values of the acceptor number (AN) of the solvent quoted in the literature are generally determined by measuring the shift in the ^{31}P NMR signal of TEPO[35] at infinite dilution as defined by:

$$AN = 2.21*(\delta_{31P,TEPO} - 41.0) \quad [14]$$

Thus, the AN is one measure of the Lewis acidity of a substance as probed via its interaction with TEPO. However, as electrolytes in Li-O_2 cells have a variety of species in them that may interact with TEPO, our first goal was to explore how the different solvent mixtures interact with the probe molecule, and to determine the sensitivity of the ^{31}P chemical shift to the different components. TEPO was added to a variety of DMSO, G4 and G1 electrolytes with varying [H_2O] and [LiTFSI], and the ANs were then estimated from the ^{31}P NMR spectra and Eq. 14 (Fig. 4 and SI Table SIII). The data in Figs. 4a–4b shows that in DMSO, increasing [LiTFSI] results in a steady increase of the ^{31}P shift of TEPO, and thus in the accepting ability of the electrolyte, both at low and high water content. By contrast, Fig. 4e shows that in G4 there is very little variation in the shift with changing [LiTFSI] remaining at approximately 57 ppm, the shift and thus the apparent value of AN being close to that of DMSO at high [LiTFSI]. Two further important observations arise from these results: i) the measured ^{31}P shift of TEPO is significantly different from that in the pure solvent (DMSO: 50.28 ppm, G4: 46.75 ppm); thus, the addition of water results in a noticeable change in the shift for G4 electrolytes, but less so for DMSO; ii) the change in ^{31}P shift of TEPO is overwhelmingly a function of [Li^+] for DMSO, with other factors having significantly less of an effect. To explore the [Li^+] relationship further a plot of the ln([Li^+]) vs the $\delta_{31P,\ TEPO}$ was made (Fig. 4f). This shows a linear relationship for DMSO and no dependence in the case of G4. This correlation is of interest, as under ideal conditions one would expect the chemical potential of Li^+—hence the Li/Li^+ couple—to be proportional to ln([Li^+]). We thus suggest that the TEPO ^{31}P shift is indirectly probing the activity of the Li^+ in solution and hence the position of the Li/Li^+ couple.

Previous studies have attributed the ^{31}P shift in glyme solvents to be a measure of the availability of Li^+ in the electrolyte.[40] This interpretation is supported by our data which shows that in G4 with 1 M of LiTFSI but without water and LiI, the ^{31}P peak was shifted to 57.12 ppm, comparable with the shift measured with the full mixture (1 M LiTFSI, 50 mM LiI, 5,000ppm H_2O). Conversely, G4 with either 50 mM LiI alone or with 5,000 ppm of water gave ^{31}P shifts of 48.99 and 50.91 ppm respectively. Further, the variation of water (0, 5,000 and 10,000 ppm) had little effect on the ^{31}P shift. Measurements were also taken of 1 M $LiNO_3$ and with 300 mM LiI instead of LiTFSI which gave similar results to those obtained with LiTFSI implying that the anion does not have a significant impact on the ^{31}P shift (Table SIII).

In G4, the ^{31}P shift is virtually invariant, with only a slight drop being seen at low [LiTFSI]. This implies a very weak bonding between Li^+ and G4, with TEPO always being able to bond to Li^+. In contrast, the ^{31}P shift in DMSO increases with increasing [LiTFSI], suggesting that TEPO must compete with DMSO for Li^+ and only with higher [LiTFSI] does TEPO bind to Li^+ for significant amounts of time. These results indicate a stronger lithium solvation ($\Delta_{sol}G(Li^+)$) for the higher DN solvent DMSO.

These results compare favourably with the work by Burke et al.[41] who reported that the ^7Li shift varied far more in G1 than in DMSO in response to changing NO_3^-:TFSI ratio, while keeping total [Li^+] constant. They suggest that NO_3^- is a better electron donor than the glyme, but not better than the DMSO, thus NO_3^- becomes incorporated into the solvation sphere in the glyme-based electrolyte, but not in DMSO. Furthermore, Leverick et al. also concluded that Li^+ is less solvated in G4 as compared to DMSO, showing a lower Li/Li^+ potential in CV experiments.[12]

^1H NMR of water.—Previous investigations into varying water concentrations in ether-based electrolyte with LiI indicated two competing effects.[16] At very low water concentrations, it is believed that water interacts directly with iodide ions. This increases the chemical shift of the water proton signal in the ^1H NMR spectrum, due to both I^--H bonding and the relativistic effects of iodine.[16] With increasing [H_2O], this effect drops off, due to there being insufficient I^- to bond to the H_2O.

In this study, the ^1H signal of water was studied in both DMSO and G4, with [H_2O] of 5,000 and 10,000 ppm and varying [LiTFSI]. For both solvents, an increase in ^1H shift, from around 3.95 ppm to 4.4 ppm, with increasing [LiTFSI] is observed (Fig. 5a). This is believed to be due to two effects: (i) water bonds directly to Li^+ and thus electron density is pulled away from the hydrogen atoms, and (ii) increasing [Li^+] helps to promote water/Li^+ clustering which increases the hydrogen bonding between water molecules. These effects are different from the shifts caused by the previously mentioned iodine interactions. In DMSO, the ^1H shift increases roughly linearly with [LiTFSI] and is virtually the same for the 5,000 and 10,000 ppm water case, whereas in G4 the 5,000 ppm water case is generally has a higher ^1H shift than the 10,000 ppm. Additionally, in G4 the change ^1H shift is not linear, with the increase in chemical shift becoming smaller with increasing [LiTFSI], and even starting to decrease for the 10,000 ppm water case. To rationalise this trend, we consider the equilibrium between water binding to Li^+ and water binding to the rest of the solvent (Eq. 15) with an equilibrium constant, K_{eq}. We consider a simplified case where these are the only two solvation environments, each with distinct ^1H shifts, and the observed ^1H shift is simply the weighted (by the amount of water in each environment) average concentration of these environments (for full derivation see "^1H NMR Model" section of the SI). We then fitted the position of the chemical shifts of these two environments and the K_{eq} to our measured data (Figs. 5e–5f).

$$K_{eq} = \frac{[H_2O \cdots Li^+][Solvent]}{[H_2O \cdots Solvent][Li^+_{(sol)}]} \quad [15]$$

We find that the trends are well explained by this simple model. For G4, the K_{eq} was found to be 56, indicating that the H_2O-Li^+ interaction is notably more favourable than the H_2O-solvent interaction. This explainsthe curvature seen in Fig. 5e, as for high [Li^+] the water is almost all bonded to Li^+, thus further additions of LiTFSI result in minimal changes. Additionally, when comparing the curves obtained for the 5,000 ppm and 10,000 ppm water cases, more LiTFSI is required before the curve flattens out for higher [H_2O], leading to a more depressed curve but with a similar shape. In contrast, for DMSO the K_{eq} was found to be 2.0 and the curve is still in a close to a linear regime suggesting that most of the water is bonded only to solvent, with the addition of more LiTFSI resulting in additional Li^+-H_2O bonding. The lack of difference between 5,000 and 10,000 ppm water in DMSO is also explained by this

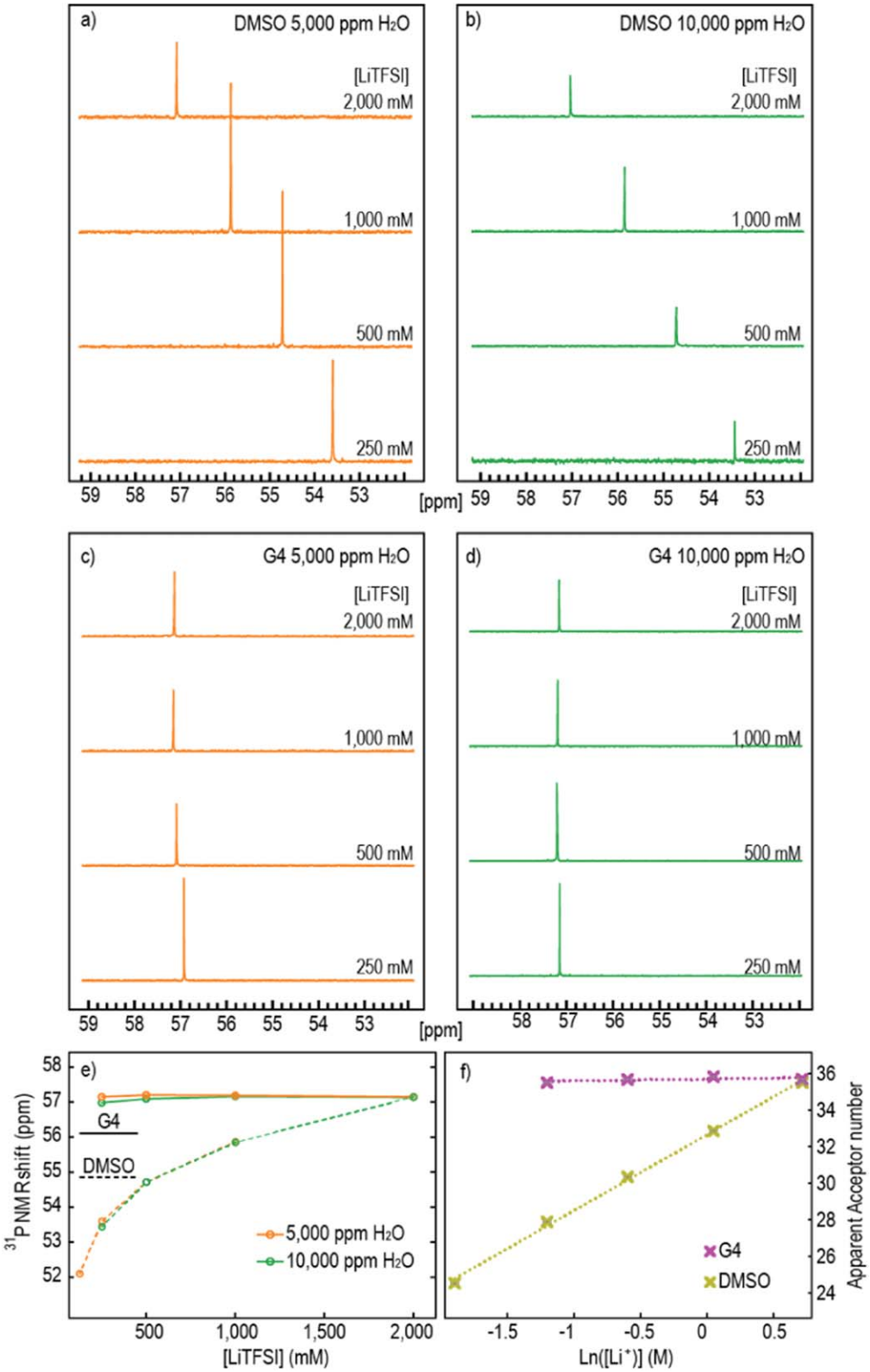

Figure 4. (a)–(d) ^{31}P NMR spectra of DMSO (5,000 and 10,000 ppm of water) and G4 (5,000 and 10,000 ppm of water) plotted as a function of [LiTFSI] (bottom to top: 250 mM, 500 mM, 1,000 mM, 2,000 mM) with 50 mM LiI. Spectra are plotted from 52 to 59 ppm showing the peak assigned to TEPO. (e) Graphs of the position of the ^{31}P peak of TEPO in DMSO (5,000 and 10,000 ppm of water) and G4 (5,000 and 10,000 ppm of water) as a function of [LiTFSI]. (f) Semi-log plot of the average AN calculated from the ^{31}P NMR shift of TEPO in 5,000 and 10,000 ppm as a function of [LiTFSI]. Vertical error bars indicate the average standard deviation between the 5,000 and 10,000 ppm cases, horizontal error bars show a 5% variation in the [LiTFSI].

model, as although additional water molecules will provide additional opportunity for water-Li^+ bonding, they also increase the total amount of water present. Thus, when most water is not bonded to Li^+, the fraction of water molecules bonded to Li^+ (and hence the weighted average ^{1}H shift) remains roughly constant between the two concentrations.

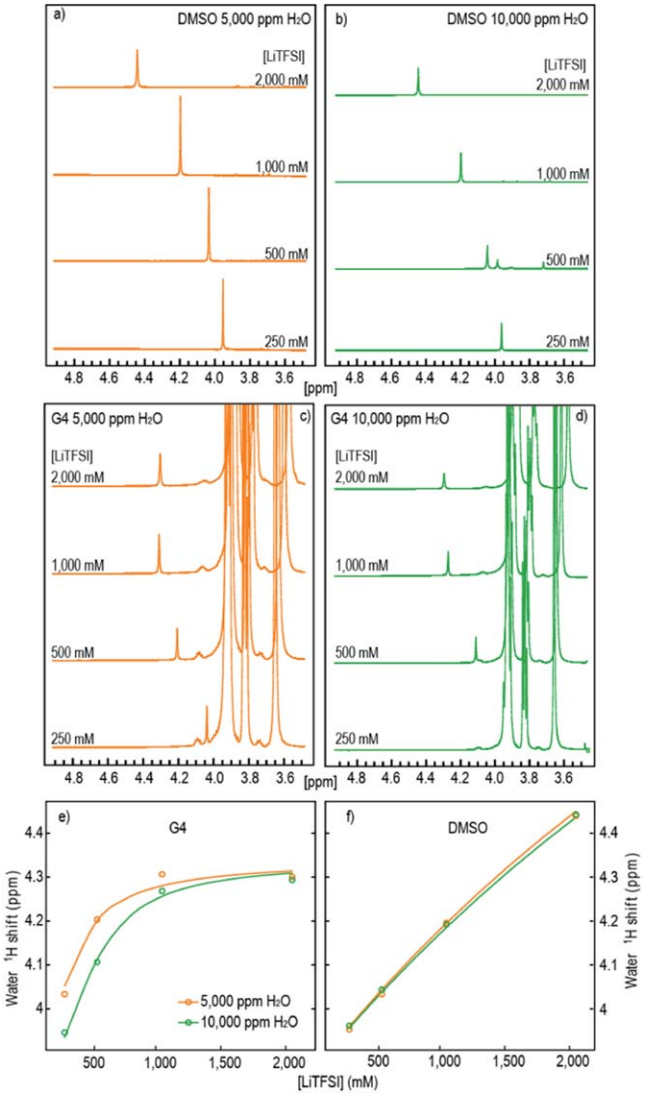

Figure 5. ^{1}H NMR spectra of DMSO (5,000 (a) and 10,000 ppm (b) of water) and G4 (5,000 (c) and 10,000 (d) ppm of water) plotted as a function of [LiTFSI] (bottom to top: 250 mM, 500 mM, 1,000 mM, 2,000 mM) with 50 mM LiI. Spectra are plotted from 3.5 to 4.9 ppm showing the peak assigned to water in DMSO as well as the protons of the glyme in G4). Additionally, graphs of the position of the ^{1}H peak of water in DMSO (5,000 and 10,000 ppm of water (f)) and G4 (5,000 and 10,000 ppm of water (e)) as a function of [LiTFSI] are shown. Lines show data fitted according to the model as described in "^{1}H NMR Model" section of the SI. The shift of the water in DMSO = 3.3 ppm and shifts of the glymes are extracted from Figures (a)–(d).

This suggests that adding LiTFSI to G4 will notably increase the water solvation energy. However, this improved solvation will only continue to a point as H_2O molecules will eventually become saturated with Li^+. This has particularly important implications in the case of LiOH-based cells, where the solvation of water becomes thermodynamically relevant (Eq. 12), suggesting that charging LiOH becomes easier (occurs at a lower potential) with increasing [LiTFSI]. In contrast, in DMSO the water solvation improves less drastically than in G4, due to water molecules having to compete with DMSO for the Li^+. The solvation of water will continue to improve to at least 2,000 mM LiTFSI and likely beyond that point due to the continued competition for Li^+ with DMSO.

This model also indicates that the water shift when not bonded to Li^+ is noticeable higher than one would expect for water in pure DMSO or G4 (the model predicting 3.87 ppm vs 3.33 ppm for trace amounts of water in DMSO, and 3.71 ppm in G4 compared to 2.46 ppm at trace amounts in the ether THF.[42] This implies that the water bonds to I^- when not bonding to Li^+, rather than bonding to the solvent, given that bonding to I^- is known to increase the water shift.[16] As this H_2O-I^- interaction must be more favourable than the interactions between water and the solvent, this provides a rationale for the observed increase in the half-wave potential of the I^-/I_3^- in G4 with increasing [H_2O], with I^- becoming better solvated. We further suggest that with increasing Li^+, water become displaced from the solvation sphere of I^- and instead bonds to the Li^+. The Li^+ then also directly interacts with I^-, improving I^- solvation. H_2O–I^- bonds do still seem to occur in DMSO, (Fig. 2b shows a slight improvement in solvation with increasing water) but are significantly weaker, likely because DMSO solvates water and I^- better than G4 does. Also given the weak interaction between water and Li^+ (relative to the solvent) in DMSO, increasing [LiTFSI] does not have the same displacing effect.

Molecular dynamics (MD) simulations.—MD simulations allow us to examine the structure of the electrolyte directly via computations. Figure 6 shows the coordination number (CN) of I^- to different species at a fixed distance (3 Å for I^-–Li^+(top), and I^-–H-OH (centre), and 5 Å for I^-–I^- (bottom)) as a function of [LiTFSI] in three different solvents. Figures S8–S18 in the SI show the full CN graphs of all of these systems, the major atom in the 1st coordination shell around the I^- being the O atom of the DMSO or the glyme. As the main interest in this work is the local environment of I^-, this is the focal point of our analysis, and in each simulation the same number of I^- atoms were used to make comparisons simpler.

Looking at the first solvation shell of I^-, (CN at 3 Å) in general the coordination of Li^+ to I^- increases as the [LiTFSI] increases (Fig. 6—top) as expected, for all solvents and water contents. However, there are noticeable differences in these trends. In neat electrolytes (blue traces), we observe a lower CN of Li^+ to I^- in DMSO compared to glymes (for a fixed [LiTFSI]), in particular to G1 at low [LiTFSI] and to G4 at high [LiTFSI]. The presence of water has a noticeable impact on DMSO-based electrolytes, increasing the CN of Li^+ to I^-. This effect is also noticeable, although slightly less markedly, in G1 electrolytes (especially at low [LiTFSI]), but in this case a higher [H_2O] increases it further, unlike in DMSO. In both glymes with 5,000 ppm of H_2O (orange traces) the CN trend plateaus at 1,000 mM LiTFSI, suggesting that the I^-–Li^+ coordination is close to saturation. This is also true for G1 with higher water content (10,000 ppm), but not for G4, which could be assigned to the formation of water clusters[16] that solvate Li^+ efficiently at lower water contents in G1 than in G4.

A look at the I^-–H_2O interaction (Fig. 6—middle) shows that as [LiTFSI] increases, H_2O is displaced out of the primary solvation shell, very noticeably in DMSO and G1, but less so in G4 and only at low [LiTFSI]. This effect seems to be independent of [H_2O] in DMSO, as was the case of the increase in coordination of Li^+ to I^-, but not in G1 where higher [H_2O] increases its coordination to I^-. This is also the case in G4, where increasing [LiTFSI] has a small effect on the I^-–H_2O interaction, with largest effect at very low concentrations.

The I^-–I^- interaction at 5 Å (in essence, a long-range structuring behaviour) shown in Fig. 6 (bottom) indicates that the three different solvents have different long-range structures around I^-, and that these structures change differently at different conditions. In DMSO-based electrolytes, there are very few I^-–I^- interactions, independent of the [LiTFSI] or [H_2O]. In water containing G1 electrolytes there is a higher chance of seeing another I^- in the solvation shell at 5 Å at low [LiTFSI], but it decreases as [LiTFSI] increases, while in neat electrolytes the I^-–I^- interactions are almost non-existent (as in the case of DMSO). The water content in G1 electrolytes has also a clear effect, with higher I^-–I^- interactions in wet electrolytes, although a maxima at 5,000 ppm of H_2O is observed, in line with previous reports from our group.[16] G4 shows a stronger iodide-related structuring as compared to the other solvents, especially at higher [LiTFSI]. Both neat and wet electrolytes display this behaviour

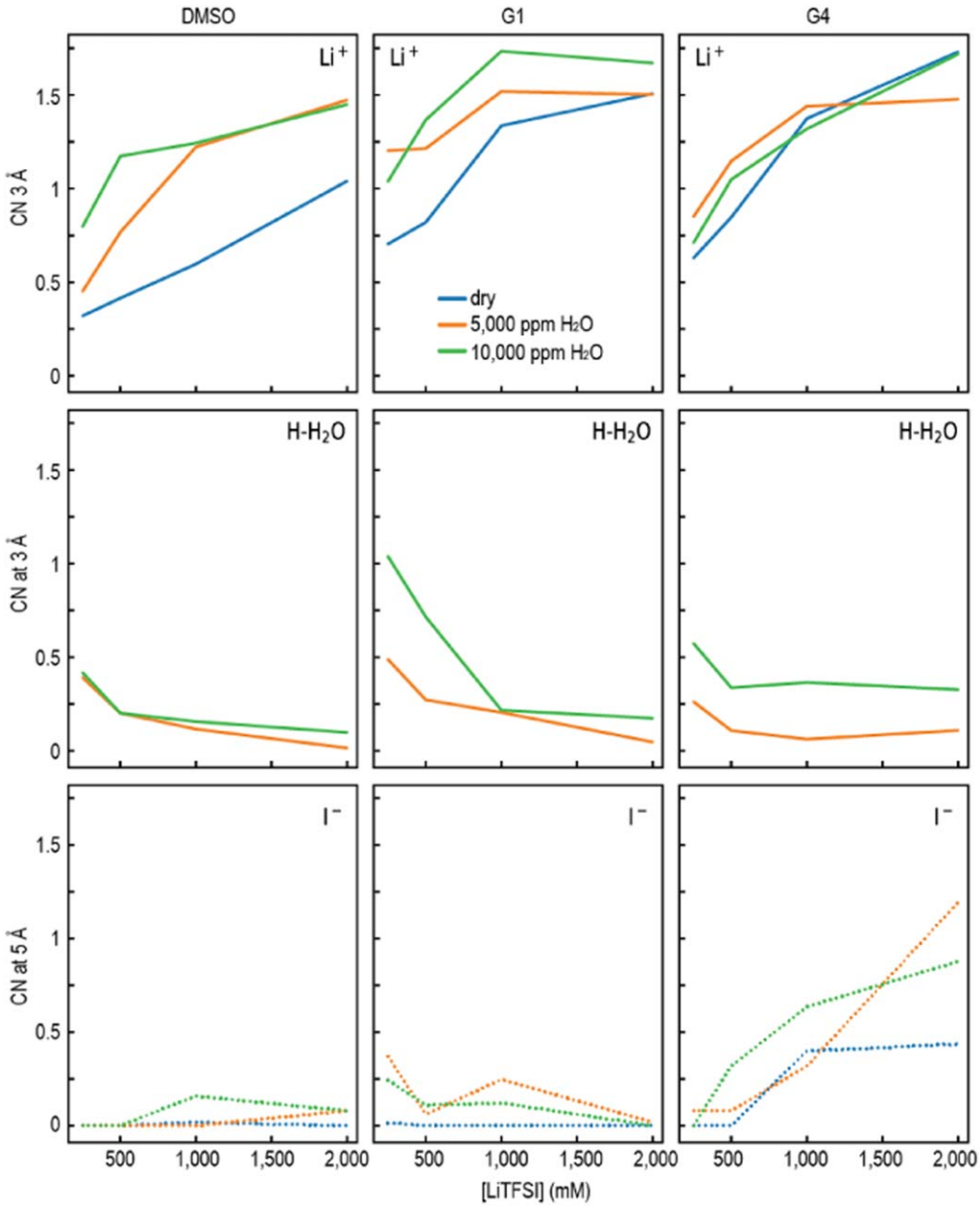

Figure 6. Coordination number (CN) of I^- to Li^+ (top) and H of water (middle), at a fixed distance (3 Å) and I^- to I^- (bottom) (with a different distance from the others (5 Å)), as a function of TFSI concentration for the three different solvent systems (left: DMSO, middle: G1, right: G4). In each graph, three water concentrations are displayed, dry, 5,000 and 10,000 ppm.

(unlike the cases of DMSO and G1 where neat electrolytes show no interaction), although high water content (10,000 ppm) shows higher influence at low [LiTFSI] and lower water content (5,000 ppm) enhancing I^-–I^- interactions to a higher degree at higher [LiTFSI]. These results indicate that the shielding of I^- (complete solvation of I^- in its first solvation shell, so I^-–I^- interactions are minimal) is highly dependent on electrolyte conditions, and this dependency is highly variable in different solvents.

These results agree with both our CV and UV absorption results where a higher solvation of I^- in DMSO to Li^+ can be inferred compared with glyme solvents (which is congruent with the polarity of the solvents and the resulting lack of ion-pairing). The ^{1}H NMR spectroscopy probed the differing interactions of water in DMSO vs glymes. To examine this, the CN of H_2O to H_2O—also measure of H-bonding between water molecules—was explored as a function of [LiTFSI] (Fig. S18). For DMSO, there seems to be a fairly even water distribution across all [LiTFSI]. While for G1, there is a higher chance of seeing water close to each other at lower [LiTFSI]. This may be due to the more polar nature of DMSO, which allows for better charge separation of ions. On the other hand, G4 has a very different behaviour, as the 2,000 mM LiTFSI shows that there is more structuring of the water. This is likely due to the very high Li^+:solvent ratio in the systems, 1:~2.3 (see Table SVII). Our UV/Vis results suggest that there is a non-uniform dispersion of water in glymes, which is in line with these results, as there are far more H_2O–H_2O interactions compared to DMSO. Furthermore, as the ^{1}H NMR showed, the data is congruent with having two solvation environments in G4, whilst DMSO has only one, which can be supported by these MD results. As noted for the ^{31}P NMR measurement of TEPO, the Li^+:solvent interaction is weaker for G4 than for DMSO. This effect can also be seen in the Li^+:solvent plots (Fig S16: Li^+:O(solvent) and Fig S17:Li^+:center-of-mass (solvent)), as the number of solvent molecules that surround Li^+ in G4 is far lower than in DMSO.

Table I. Overview of the methods used to probe solvation.

UV/Vis	*Strength:* Probes an electronic transition that is related to the solvation environment. High throughput. Sensitive to cations and solvent. *Limitation:* Challenging to interpret. Probes the energy of the excited state and thus difficult to deconvolute specific effects.
NMR (^{1}H)	*Strength:* Probes the local proton environment. *Limitation:* Probes the local proton environment. Chemical shift timescale is slow in cf to UV/Vis and IR (ms): spectra measure the average local environments for liquids. Can be challenging to interpret.
NMR (^{31}P)	*Strength:* Forms the basis of the determination of the AN. Our work shows it to be a strong measure of Li^{+} binding. *Limitation:* Requires an additional molecule in the solution to probe the electrolyte.
MD	*Strength:* Local coordination structure can be revealed directly. Time evolution of the system is accessible on the nanoscale. *Limitation:* Force fields are not always available for all components of the system. Requires experimental corroboration. Reactions are challenging. Calculations can become quite large and involved, requiring significant computational resources.
CV	*Strength:* Direct measure of the electrochemical properties that can be affected by the solvation. *Limitation:* Need other experimental data/theory to interpret trends.

Discussion

From a thermodynamics point of view, we can see that $E(RM^{red}/RM^{ox})$ will affect the driving force of the OER in Li-O_2 cells (Eq. 8). When using I^-/I_3^- as a RM this couple is heavily influenced by the solvation environment of I^- and Li^+. A suite of complementary techniques was used to build a comprehensive picture of the iodide solvation environment, where each individual method is an indirect probe, sensitive to different factors that may affect the I^- and Li^+ solvation and subsequently the redox potential. The experimental methods used here, UV/Vis and NMR (both ^1H and ^{31}P) indirectly probe the solvation environments, while MD simulations provide coordination information of the I^- to various electrolyte components. The strengths and limitations of each technique used in this paper are summarized in Table I.

The different aspects of the I^- solvation revealed by each technique are now discussed in relation to the measured I^-/I_3^- couple redox potentials. The CV data are a direct measure of I^-/I_3^- couple redox potential and hence of the change in activity due to mediator solvation. In G4, increasing [H_2O] and/or [LiTFSI] increases $E(I^-/I_3^-)$, while in DMSO [H_2O] and [LiTFSI] have a limited effect (Fig. 2). This is ascribed to improved solvation of I^- in DMSO. UV/Vis probes the electronic transitions associated with the solvation environment of I^-. In G4 and G1 increasing [H_2O] and/or [LiTFSI] gives rise to a discrete new absorption at 230 nm which we ascribe to an environment with increased I^- solvation (Fig. 3). This is consistent with an increase in the $\Delta_{sol}G(RM^{red}) - \Delta_{sol}G(RM^{ox})$ term as seen in the CV measurements. In DMSO, increasing [H_2O] and [LiTFSI] has less of an effect on the UV signals indicating less of an effect on the I^- solvation (Fig. 3), consistent with the essentially constant $E(I^-/I_3^-)$ couple. The MD results, (Fig. 6), similarly indicate that the I^-–I^- CN is very low and shows little to no change with increasing [LiTFSI] or [H_2O] in DMSO electrolytes.

^{31}P NMR of the molecule TEPO in various electrolyte compositions was shown to probe the solvation of Li^+ and hence (indirectly) probe the Li/Li^+ (stripping and plating) couple. In G4, Li^+ is weakly solvated by the electrolyte and is always able to bond to TEPO, giving rise to a constant ^{31}P shift that does not vary with water or Li^+ concentration over a wide range of concentrations (Fig. 4). In DMSO, there is a competition between TEPO and DMSO for the Li^+—and with increased [LiTFSI], more Li^+ is available to bind to TEPO and the ^{31}P shift increases. Furthermore, the increased solvation of Li^+ by DMSO, results in a competitive binding process between DMSO, TEPO and water. The implications here for the Li/Li^+ couple, namely that Li^+ is better solvated in DMSO resulting in a more negative Li/Li^+ couple, are consistent with the literature.[12] Note that the variation in the Li/Li^+ couple between solvents (and indeed different water concentrations) means that a comparison between redox mediators in different solvents requires the use of a three-electrode cell.

The ^1H NMR data show that water bonds strongly to Li^+ in both G4 and DMSO (Fig. 4), the water-Li^+ interaction being more favorable in G4 than in DMSO as expected. The competitive binding between solvent and water, and the stronger solvation of Li^+ in DMSO vs G4 (water is also better solvated in DMSO) means that a higher concentration of Li^+ is needed in DMSO before the shift of water approaches that seen in G4. A simple equilibrium model is developed (see SI and Eq. 15) that considers the equilibrium between water binding to Li^+ and water binding to the rest of the solvent (Eq. 15), which provides an excellent fit to the NMR data and confirms that Li^+-water interactions are much stronger in G4 vs DMSO. The approach will prove useful to model water shifts in other electrolyte systems, e.g.,[16] which are often difficult to rationalise due to competing interactions.

The strong I^--H_2O interaction is of particular relevance to LiOH-based Li-O_2 cells and the strong I^--H_2O interaction inferred from our data, in G4-based electrolytes in particular indicates that the interplay between the activities of H_2O, Li^+, and I^- should be considered when optimising the OER process during charge of LiOH-based cells.

Finally, further information about the electrolyte structure can be gained by using additional techniques. Raman and IR can probe bonding directly and thus give information on some aspects of the electrolyte structure. Additionally, it may be possible to verify MD simulations using neutron scattering, particularly small angle neutron scattering to investigate the outer coordination shells and the predicted clustering.[43,44] As for the computational aspect, ideally future work should include direct calculations of electronic energy levels, such as absorption spectra. However, as we have shown, the composition of the electrolyte does give rise to complex interrelated interactions and to capture them in ab initio calculations will be challenging. The focus of this work is to highlight the importance of the RM solvation environment and to investigate suitable techniques to probe this. The interplay between the factors dictating the solvation of RM species discussed above is complex and dependent on the nature of the electrolyte, as our data indicates. This is reflected in the considerable scatter in the I^-/I_3^- redox potential observed for both DMSO and glyme-based electrolytes shown in Figs. 1 and S1, where neither [Li^+], nor the AN/DN of the solvent are clear indicators of its position.

Conclusions

Previous studies have investigated the variation in redox potentials of RMs in different electrolytes but have tended to focus on one aspect such as AN, or [Li^+]. In our most recent work, we showed that the interplay between two additives (water and an ionic liquid), added to an iodide-mediated electrolyte, was complex and had strong effects on the solvation of I^-. This in turn influenced its electrochemical behaviour, to the point of completely changing the charge mechanism of the cell.[15] Here, we explore further this complex interplay as a function of solvent, salt concentration, and water concentration. A thermodynamic analysis highlights the dependence of the redox potentials on solvation environments of the RMs, which we examine with CV, UV/Vis, NMR, and MD simulations, each probing different solvation aspects of the electrolyte. Our results show that both water and Li^+ ions affect the solvation environments differently in the three solvents studied. In general, ion-pairs are more closely associated in glyme-based electrolytes than in DMSO-based electrolytes, which translates into a marked increase in the half-wave potential of the I^-/I_3^- redox couple in G4-based electrolytes with increasing [Li^+], while it remains almost constant in DMSO-based electrolytes. Additionally, added water appears to have less of an effect on the CV, UV/Vis and ^1H NMR measurements in DMSO.

As each technique probes different solvation interactions, a more holistic approach is needed to obtain a more complete picture of the solvation of the species in solution, which is inherently a highly multidimensional problem. This in turn will allow for better rationalisation of the observed trends in the thermodynamics of the mediator, as a detailed characterization of the local electrolyte structures can then help explain the scatter in redox potentials observed in the literature and our own CVs. The ability to tune RMs for lower overpotentials and optimize the electrolyte for highly reversible Li-air batteries requires a systematic and complete investigation as discussed above and can build upon this work. Work expanding the set of electrolytes and techniques used in this study will be performed in the future, thus providing a better understanding of RM behaviour and ultimately leading to improved Li-air batteries.

Acknowledgments

JHJE, EJ and CPG were supported by EC H2020 grant no. 835073 (ERC Advanced Investigator Grant for Prof. Clare Grey). IT and CPG were supported by EPSRC grant no.s EP/P003532/1 and

EP/M009521/1 DJR00640. EW is grateful to the Cambridge Trust for a Cambridge International Scholarship. VK was supported by the BBSRC DTP. The computational work was performed using resources provided by the Cambridge Service for Data Driven Discovery (CSD3) operated by the University of Cambridge Research Computing Service (www.csd3.cam.ac.uk), provided by Dell EMC and Intel using Tier-2 funding from EPSRC capital grant no. EP/P020259/1) and DiRAC funding from the Science and Technology Facilities Council (www.dirac.ac.uk).

ORCID

Erlendur Jónsson https://orcid.org/0000-0002-7776-0484
James H. J. Ellison https://orcid.org/0000-0002-4578-5804
Evelyna Wang https://orcid.org/0000-0002-5697-474X
Israel Temprano https://orcid.org/0000-0001-5610-8908
Clare P. Grey https://orcid.org/0000-0001-5572-192X

References

1. G. Girishkumar, B. McCloskey, A. C. Luntz, S. Swanson, and W. Wilcke, "Lithium-air battery: promise and challenges." *J. Phys. Chem. Lett.*, **1**, 2193 (2010).
2. D. Aurbach, B. D. McCloskey, L. F. Nazar, and P. G. Bruce, "Advances in understanding mechanisms underpinning lithium-air batteries." *Nat. Energy*, **1**, 16128 (2016).
3. W. J. Kwak et al., "Lithium–Oxygen Batteries and Related Systems: Potential, Status, and Future." *Chemical Reviews*, **120**, 6626 (2020).
4. T. Liu, J. P. Vivek, E. W. Zhao, J. Lei, N. Garcia-Araez, and C. P. Grey, "Current challenges and routes forward for nonaqueous lithium-air batteries." *Chem. Rev.*, **120**, 6558 (2020).
5. A. Bose Styczynski and L. Hughes, "Public policy strategies for next-generation vehicle technologies: an overview of leading markets." *Environmental Innovation and Societal Transitions*, **31**, 262 (2019).
6. J. Meckling and J. Nahm, "The politics of technology bans: industrial policy competition and green goals for the auto industry.." *Energy Policy*, **126**, 470 (2019).
7. J. B. Park, S. H. Lee, H. G. Jung, D. Aurbach, and Y. K. Sun, "Redox mediators for Li–O_2 batteries: status and perspectives." *Adv. Mater.*, **30**, 1704162 (2018).
8. W.-J. Kwak, H. Kim, H.-G. Jung, D. Aurbach, and Y.-K. Sun, "Review—a comparative evaluation of redox mediators for Li-O_2 batteries: a critical review." *J. Electrochem. Soc.*, **165**, A2274 (2018).
9. B. J. Bergner, A. Schürmann, K. Peppler, A. Garsuch, and J. Janek, "TEMPO: a mobile catalyst for rechargeable Li-O_2 batteries." *JACS*, **136**, 15054 (2014).
10. X. Gao, Y. Chen, L. R. Johnson, Z. P. Jovanov, and P. G. Bruce, "A rechargeable lithium-oxygen battery with dual mediators stabilizing the carbon cathode." *Nat. Energy*, **2**, 17118 (2017).
11. T. Liu, M. Leskes, W. Yu, A. J. Moore, L. Zhou, P. M. Bayley, G. Kim, and C. P. Grey, "Cycling Li-O_2 Batteries via LiOH formation and decomposition." *Science*, **350**, 530 (2015).
12. G. Leverick, M. Tułodziecki, R. Tatara, F. Bardé, and Y. Shao-Horn, "Solvent-dependent oxidizing power of LiI redox couples for Li-O_2 batteries." *Joule*, **3**, 1106 (2019).
13. A. Nakanishi, M. L. Thomas, H. M. Kwon, Y. Kobayashi, R. Tatara, K. Ueno, K. Dokko, and M. Watanabe, "Electrolyte composition in Li/O_2 Batteries with LiI redox mediators: solvation effects on redox potentials and implications for redox shuttling." *J. Phys. Chem. C*, **122**, 1522 (2018).
14. V. Pande and V. Viswanathan, "Criteria and considerations for the selection of redox mediators in nonaqueous Li-O_2 batteries." *ACS Energy Lett.*, **2**, 60 (2017).
15. I. Temprano, T. Liu, E. Petrucco, J. H. J. Ellison, G. Kim, E. Jónsson, and C. P. Grey, "Toward reversible and moisture-tolerant aprotic lithium-air batteries." *Joule*, **4**, 2501 (2020).
16. T. Liu, G. Kim, E. Jónsson, E. Castillo-Martinez, I. Temprano, Y. Shao, J. Carretero-González, R. N. Kerber, and C. P. Grey, "Understanding LiOH formation in a Li-O_2 battery with LiI and H_2O additives." *ACS Catal.*, **9**, 66 (2019).
17. C. M. Burke, R. Black, I. R. Kochetkov, V. Giordani, D. Addison, L. F. Nazar, and B. D. McCloskey, "Implications of 4 e^- oxygen reduction via iodide redox mediation in Li-O_2 batteries." *ACS Energy Lett.*, **1**, 747 (2016).
18. Y. G. Zhu et al., "Proton enhanced dynamic battery chemistry for aprotic lithium-oxygen batteries." *Nat. Commun.*, **8**, 14308 (2017).
19. Y. Qiao, S. Wu, Y. Sun, S. Guo, J. Yi, P. He, and H. Zhou, "Unraveling the complex role of iodide additives in Li-O_2 batteries." *ACS Energy Lett.*, **2**, 1869 (2017).
20. C. Zhang, N. Dandu, S. Rastegar, S. N. Misal, Z. Hemmat, A. T. Ngo, L. A. Curtiss, and A. Salehi-Khojin, "A comparative study of redox mediators for improved performance of Li–oxygen batteries." *Adv. Energy Mater.*, **10**, 2000201 (2020).
21. W. J. Kwak et al., "Understanding the behavior of Li-oxygen cells containing LiI." *J. Mater. Chem. A*, **3**, 8855 (2015).
22. M. Yu, X. Ren, L. Ma, and Y. Wu, "Integrating a redox-coupled dye-sensitized photoelectrode into a lithium–oxygen battery for photoassisted charging." *Nat. Commun.*, **5**, 5111 (2014).
23. L. Martinez, R. Andrade, E. G. Birgin, and J. M. Martinez, "Software news and updates PACKMOL: a package for building initial configurations for molecular dynamics simulations." *J. Comput. Chem.*, **30**, 2157 (2009).
24. J. N. C. Lopes and A. A. H. Pádua, "Molecular force field for ionic liquids composed of triflate or bistriflylimide anions." *J. Phys. Chem. B*, **108**, 16893 (2004).
25. C. Caleman, P. J. Van Maaren, M. Hong, J. S. Hub, L. T. Costa, and D. Van Der Spoel, "Force field benchmark of organic liquids: density, enthalpy of vaporization, heat capacities, surface tension, isothermal compressibility, volumetric expansion coefficient, and dielectric constant.." *J. Chem. Theory Comput.*, **8**, 61 (2012).
26. M. J. Abraham, T. Murtola, R. Schulz, S. Páll, J. C. Smith, B. Hess, and E. Lindah, "Gromacs: high performance molecular simulations through multi-level parallelism from laptops to supercomputers.." *SoftwareX*, **1–2**, 19 (2015).
27. T. Liu, G. Kim, J. Carretero-González, E. Castillo-Martínez, and C. P. Grey, "Response to comment on 'cycling Li-O_2 batteries via LiOH formation and decomposition." *Science*, **352**, 667 (2016).
28. C. L. Bentley, A. M. Bond, A. F. Hollenkamp, P. J. Mahon, and J. Zhang, "Voltammetric determination of the iodide/iodine formal potential and triiodide stability constant in conventional and ionic liquid media.." *J. Phys. Chem. C*, **119**, 22392 (2015).
29. M. Blandamer, T. Gough, and M. Symons, "Solvation spectra. Part 11.—cation dependence of the ultra-violet absorption spectra of iodide ions in solvents of low polarity." *Trans. Faraday Soc.*, **62**, 286 (1966).
30. S. E. Bradforth and P. Jungwirth, "Excited states of iodide anions in water: a comparison of the electronic structure in clusters and in bulk solution." *J. Phys. Chem. A*, **106**, 1286 (2002).
31. M. Smith and M. Symons, "Solvation Spectra. Part II.—the nature of the electronically excited state of solvated iodide ions." *Trans. Faraday Soc.*, **54**, 346 (1958).
32. T. Griffiths and M. Symons, "Solvation Spectra. Part III.—further studies of the effect of environmental changes on the ultra-violet spectrum of iodide ions." *Trans. Faraday Soc.*, **56**, 1125 (1960).
33. I. Landa-Medrano, M. Olivares-Marín, R. Pinedo, I. Ruiz de Larramendi, T. Rojo, and D. Tonti, " Operando UV-visible spectroscopy evidence of the reactions of iodide as redox mediator in Li–O_2 batteries." *Electrochem. Commun.*, **59**, 24 (2015).
34. T. Griffiths and R. Wijayanayake, "Effects of cations upon absorption spectra. Part V.—charge-transfer-to-solvent spectrum of iodide and ion-pair formation." *Trans. Faraday Soc.*, **66**, 1563 (1970).
35. U. Mayer, V. Gutmann, and W. Gerger, "The acceptor number - a quantitative empirical parameter for the electrophilic properties of solvents." *Monatsh. Chem.*, **106**, 1235 (1975).
36. D. G. Kwabi, V. S. Bryantsev, T. P. Batcho, D. M. Itkis, C. V. Thompson, and Y. Shao-Horn, "Experimental and computational analysis of the solvent-dependent O_2/Li^+-O_2^- redox couple: standard potentials, coupling strength, and implications for lithium-oxygen batteries." *Angewandte Chemie - International Edition*, **55**, 3129 (2016).
37. N. B. Aetukuri, B. D. McCloskey, J. M. Garciá, L. E. Krupp, V. Viswanathan, and A. C. Luntz, "Solvating additives drive solution-mediated electrochemistry and enhance toroid growth in non-aqueous Li-O_2 batteries." *Nat. Chem.*, **7**, 50 (2015).
38. H. D. Lim, B. Lee, Y. Bae, H. Park, Y. Ko, H. Kim, J. Kim, and K. Kang, "Reaction chemistry in rechargeable Li-O_2 batteries." *Chem. Soc. Rev.*, **46**, 2873 (2017).
39. L. Wang, Y. Zhang, Z. Liu, L. Guo, and Z. Peng, "Understanding oxygen electrochemistry in aprotic Li–O_2." *Batteries. Green Energy and Environment*, **2**, 186 (2017).
40. D. J. Eyckens and L. C. Henderson, "A review of solvate ionic liquids: physical parameters and synthetic applications." *Frontiers in Chemistry*, **7**, 1 (2019).
41. C. M. Burke, V. Pande, A. Khetan, V. Viswanathan, and B. D. McCloskey, "Enhancing electrochemical intermediate solvation through electrolyte anion selection to increase nonaqueous Li–O_2 battery capacity." *Proc. Natl. Acad. Sci. U.S.A.*, **112**, 9293 (2015).
42. G. R. Fulmer, A. J. M. Miller, N. H. Sherden, H. E. Gottlieb, A. Nudelman, B. M. Stoltz, J. E. Bercaw, and K. I. Goldberg, "NMR chemical shifts of trace impurities: common laboratory solvents, organics, and gases in deuterated solvents relevant to the organometallic chemist." *Organometallics*, **29**, 2176 (2010).
43. S. Saito et al., "Li^+ local structure in li-tetraglyme solvate ionic liquid revealed by neutron total scattering experiments with the $^{6/7}$Li isotopic substitution technique." *J. Phys. Chem. Lett.*, **7**, 2832 (2016).
44. K. Shimizu et al., "Structural and aggregate analyses of (Li salt + glyme) mixtures: the complex nature of solvate ionic liquids." *Phys. Chem. Chem. Phys.*, **17**, 22321 (2015).